

Scale-dependent homogenization of random composites as micropolar continua

Patrizia Trovalusci^{a,*}, Martin Ostoja-Starzewski^b, Maria Laura De Bellis^a, Agnese Murralli^a

^a*Department of Structural and Geotechnical Engineering,
Sapienza, University of Rome, via A. Gramsci 53, 00197 Rome, Italy*

^b*Department of Mechanical Science and Engineering,
Institute for Condensed Matter Theory and Beckman Institute,
University of Illinois at Urbana-Champaign, Urbana, IL 61801, USA*

Abstract

A multitude of composite materials ranging from polycrystals to rocks, concrete, and masonry overwhelmingly display random morphologies. While it is known that a Cosserat (micropolar) medium model of such materials is superior to a Cauchy model, the size of the Representative Volume Element (RVE) of the effective homogeneous Cosserat continuum has so far been unknown. Moreover, the determination of RVE properties has always been based on the periodic cell concept. This study presents a homogenization procedure for disordered Cosserat-type materials without assuming any spatial periodicity of the microstructures. The setting is one of linear elasticity of statistically homogeneous and ergodic two-phase (matrix-inclusion) random microstructures. The homogenization is carried out according to a generalized Hill-Mandel type condition applied on mesoscales, accounting for non-symmetric strain and stress as well as couple-stress and curvature tensors. In the setting of a two-dimensional elastic medium made of a base matrix and a random distribution of disk-shaped inclusions of given density, using Dirichlet-type and Neumann-type loadings, two hierarchies of scale-dependent bounds on classical and micropolar elastic moduli are obtained. The characteristic length scales of approximating micropolar continua are then determined. Two material cases of inclusions, either stiffer or softer than the matrix, are studied and it is found that, independent of the contrast in moduli, the RVE size for the bending micropolar moduli is smaller than that obtained for the classical moduli. The results point to the need of accounting for: spatial randomness of the medium, the presence of inclusions intersecting the edges of test windows, and the importance of additional degrees of freedom of the Cosserat continuum.

Keywords:

random microstructure, homogenization, Cosserat, finite-size-scaling, RVE, composites

*Corresponding author

Email address: patrizia.trovalusci@uniroma1.it (Patrizia Trovalusci)

1. Introduction and setting of the problem

A wide range of composite materials, used in different engineering fields or present in nature, display non-periodic arrangement of the constituents. Referring to particulate composites made of particles (inclusions) embedded in dissimilar matrices, examples are polymer, ceramic, metal matrix composites (Fig. 1, a, b), but also granular materials, concrete, masonry made of crushed stones casually arranged in the mortar and even porous rocks (Fig. 1, c, d).

The evaluation of the effective mechanical response of such materials cannot disregard the spatial randomness markedly characterizing the disposition of the inclusions. Within this framework, an interesting challenge, motivated by the needs of preservation and restoration of the architectural heritage of many countries is the study of ancient masonry. This material can be regarded as a particulate composite generally characterized by spatial randomness, unlike the current masonry in which the disposition of the constituents is mainly periodic. Referring to masonry-like materials, while periodic stonework masonry attracted the interest of several researches in the past decades, a comprehensive understanding of the mechanical behaviour of such random assemblies is still lacking.

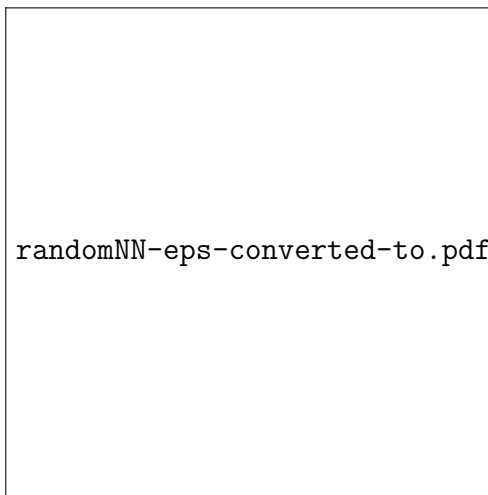


Figure 1: Particulate random composites. a, b: ceramic/metal matrix composites ; c, d: Roman concrete, tuffaceous rock.

For many years, periodically structured masonries have been effectively modeled as anisotropic continua by adopting standard homogenization techniques, obtaining satisfactory results using micromorphic continua modeling (De Bellis and Addessi, 2011; Bacigalupo and Gambarotta, 2011; Addessi and Sacco, 2012), also resorting to coarse-graining approaches based on discrete-continuum modeling (Ortiz and Phillips, 1999; Trovalusci et al., 2008, 2010; Trovalusci, 2014), and addressing the non-linear behaviours

(Trovalusci and Masiani, 2003, 2005; Sansalone and Trovalusci, 2010). Micropolar continua approaches accounting for the effects of material internal lengths and, in particular, non-symmetries of the strain and stress tensors have turned out to be more effective than the local and second gradient continua approaches (Pau and Trovalusci, 2011; Trovalusci and Pau, 2014).

More recently, various procedures have also been proposed to perform classical homogenization for non-periodic masonry assemblies. In the work (Zeman and Šejnoha, 2007) for instance, a notion of statistically equivalent periodic unit cell, accounting for the geometrical randomness of various material systems, is introduced in order to derive the homogenized effective properties. In the article (Gusella and Cluni, 2006) instead, the authors consider masonry assemblies characterized by random geometrical and constitutive properties and use windows of varying size for defining the minimum size of a representative volume element for the homogenization process. In the work (Spence et al., 2008), two random fields, one associated with the stone geometry and another representing the global morphology, are adopted in order to simulate the realizations of an actual random masonry wall by means of a statistical algorithm. In the article (Cecchi and Sab, 2009), non-periodic masonry is studied aiming for evaluating the effect of a random perturbation on the elastic material response. In another work (Milani and Lourenço, 2010), a rigid-plastic homogenization model for the limit analysis of masonry walls made of blocks of various size randomly assembled and out-of-plane loaded is presented. Finally, in the article (Cavalagli et al., 2011) the non-periodicity of masonry structures is taken into account in order to define a strength domain in generalized plane strain state.

Usually, homogenization techniques for random media are based on the solution of boundary value problems (BVPs) over finite-size mesoscales (Terada et al., 2000; Kanit et al., 2003; Sab and Nedjar, 2005; Gitman et al., 2007; Hatami-Marbini and Picu, 2009; Ghosh, 2011; Salmi et al., 2012). In order to account for the effects of the microstructural size, heterogeneous non-periodic materials have been also studied by extending the homogenization schemes to gradient-enhanced continua, applied to a single fixed mesoscale (Kouznetsova et al., 2002, 2004). To the best of our knowledge, however, finite-size-scaling homogenization techniques have never been applied to random non-classical materials and, in particular, to continua with additional degrees of freedom (Capriz, 1989; Eringen, 1999). In this framework, the non-periodic masonry becomes an opportunity to develop a general strategy for dealing with composite random media which are described as micropolar continua (Nowacki, 1970, 1986; Eringen, 1999), in order to take into account size effects and non symmetric behaviour.

The key issue in the homogenization theories for random materials is that the basic concept of Representative Volume Element (RVE), well established in homogenization of periodic media, requires the adoption of very large (theoretically infinite) material domains; depending on the macroscopic body size, this may invalidate the scale separation commonly assumed in continuum mechanics (Ostoja-Starzewski, 1998, 2006). These and related concepts have been widely studied within the framework of elastic, plastic, thermoelastic and permeable random microstructures in (Ostoja-Starzewski et al., 2007;

Khisaeva and Ostoja-Starzewski, 2006; Ostoja-Starzewski, 2008, 2011). According to these studies, stochastic approaches can be used to perform homogenization of materials with random microstructure approaching the minimum RVE size as convergence value of two hierarchies of bounds stemming from the solutions of Dirichlet and Neumann BVPs. In particular, under the assumption that the medium is characterized by statistical homogeneity and mean-ergodicity, Statistical Volume Elements (SVEs) can be set up on a mesoscale, i.e. any finite scale relative to the microstructural length scale, on which both Dirichlet and Neumann BVPs can be solved. On that basis, two scale dependent hierarchies of mesoscale bounds for the effective material properties can be obtained. The convergence trend, as the SVE increases, allows one to approximate the RVE size and to estimate the effective constitutive moduli of the random composites.

Following the above mentioned approach, in this paper we develop a homogenization procedure which applies to random composites perceived as Cosserat continua both at the micro and macro level. The use of a Cosserat continuum at the local level is appropriate when the size of a heterogeneity is comparable to the characteristic length of its inner microstructure. In this framework, it is possible to account for local bending deformation mechanisms, which can be prominent in the presence of voids of size comparable to the heterogeneity size (e.g. nano-crystals, defected or cellular materials, etc.) (Forest et al., 1999, 2001; Onck, 2002). Here we want to define a general description, able to represent a wide range of materials characterized by different ratios between the above mentioned scales. The classical description (Cauchy) can be obtained as a limit case in which the characteristic length is very small, compared to the heterogeneity size. This approach requires macrohomogeneity conditions generalized to micropolar continua (Li and Liu, 2009; Liu, 2013) which hold also in the case of spatial non-periodicity (Ostoj-Starzewski, 2011). As the first step, the linear-elastic case is taken into account, thus providing an estimate of the elastic coefficients of the micropolar continuum. In particular, at the microlevel each phase is isotropic while at the macrolevel the equivalent continuum of any specific realization is generally anisotropic.

Among various parameters that may randomly vary in a particle composite, such as position, size, shape, density of inclusions as well as mechanical properties of the constituents, here we focus on the spatially random distribution of inclusions in a homogeneous matrix. We consider a simplified micromodel of an elastic two-phase composite, made of a base matrix with randomly distributed circular inclusions of a fixed radius and fixed nominal volume fraction. We take into account two cases characterized by different contrasts between material phases. As a measure of the contrast, the following variables are taken into account: the ratio between Young's moduli of the inclusions and matrix (E^i/E^m) and ratio between the (micropolar) characteristic lengths of the inclusions and matrix (l_c^i/l_c^m). Thus, case (a) is a material in which stiff aggregates are surrounded by a softer mortar matrix ($E^i/E^m = 6$; $l_c^i/l_c^m = 10$), and case (b) is a material in which soft inclusions are embedded in a stiffer matrix ($E^i/E^m = 0.167$; $l_c^i/l_c^m = 0.1$), Fig. 2.

The paper is organized as follows. In Sec. 2 the balance, compliance and constitutive equations for a Cosserat medium are presented and the generalized macrohomogeneity



Figure 2: Two cases of material contrast studied (inclusion/matrix): (a) higher contrast material; (b) lower contrast material.

condition as well the relative Dirichlet and Neumann boundary value conditions to be imposed on the test window are explained in detail. Sec. 3.1 is devoted to the description of the stochastic procedure proposed for the estimation of the overall classical and micropolar moduli and to detect the RVE size. In Sec. 3.2 the numerical results for determining the convergence trends of the elastic homogenized moduli of the two material cases (a) and (b) are reported and discussed. Finally, in Sec. 4 some final remarks concerning the suitability of the statistical approach applied to classical and non-classical continua are presented and discussed.

2. Macrohomogeneity condition in micropolar media

Under consideration is a heterogeneous (two-phase) micropolar linear elastic continuum in quasi-static setting. Given the micropolar character, the kinematical descriptors of each material point are displacement and rotation vectors (u_i) and (φ_i), $i = 1, 3$. Within the framework of a linearized theory, the kinematics of this continuum is governed by:

$$\gamma_{ij} = u_{i,j} + e_{kij}\varphi_k, \quad \kappa_{ij} = \varphi_{i,j}, \quad (1)$$

where (γ_{ij}) and (κ_{ij}) are the strain and curvature tensors, respectively. In Eq. (1) and in the equations below (e_{ijk}) is the Levi-Civita tensor, and the indices vary as $i, j, k = 1, 3$.

The balance equations in the absence of body forces and couples are:

$$\tau_{ij,j} = 0, \quad \mu_{kj,j} + e_{kji}\tau_{ij} = 0, \quad (2)$$

where (τ_{ij}) and (μ_{ij}) are respectively the stress and couple stress tensors. Denoting by (t_i) and (m_i) the tractions and surface couples on the boundary of a control volume of outward normal (n_i), we also have:

$$t_i = \tau_{ij} n_j, \quad m_i = \mu_{ij} n_j. \quad (3)$$

In order to separately investigate the classical and micropolar components, we divide the strain and stress tensors into their symmetric and skew-symmetric part:

$$\gamma_{ij} = \varepsilon_{ij} + \alpha_{ij}, \quad \tau_{ij} = \sigma_{ij} + \beta_{ij}, \quad (4)$$

where $\varepsilon_{ij} = \frac{1}{2}(u_{i,j} + u_{j,i})$, $\alpha_{ij} = \frac{1}{2}(u_{i,j} - u_{j,i}) - e_{kij}\varphi_k$, while $\sigma_{ij} = \frac{1}{2}(\tau_{ij} + \tau_{ji})$, $\beta_{ij} = \frac{1}{2}(\tau_{ij} - \tau_{ji})$

In the sequel we consider a two-dimensional (2D) micropolar continuum in which the independent strain and stress components are ordered into the vectors:

$$\begin{aligned} \{\varepsilon\} &= \{\varepsilon_{11} \quad \varepsilon_{22} \quad \varepsilon_{12}\}^T & \{\sigma\} &= \{\sigma_{11} \quad \sigma_{22} \quad \sigma_{12}\}^T \\ \{\alpha\} &= \{\alpha_{12}\} & \{\beta\} &= \{\beta_{12}\} \\ \{\kappa\} &= \{\kappa_{31} \quad \kappa_{32}\}^T & \{\mu\} &= \{\mu_{31} \quad \mu_{32}\}^T. \end{aligned} \quad (5)$$

The stress–strain relations for a 2D linear elastic isotropic micropolar material can then be written as:

$$\begin{bmatrix} \sigma_{11} \\ \sigma_{22} \\ \sigma_{12} \\ \beta_{12} \\ \mu_{31} \\ \mu_{32} \end{bmatrix} = \begin{bmatrix} \lambda + 2\mu & \lambda & 0 & 0 & 0 & 0 \\ \lambda & \lambda + 2\mu & 0 & 0 & 0 & 0 \\ 0 & 0 & 2\mu & 0 & 0 & 0 \\ 0 & 0 & 0 & -2\mu_c & 0 & 0 \\ 0 & 0 & 0 & 0 & 2\mu l_c^2 & 0 \\ 0 & 0 & 0 & 0 & 0 & 2\mu l_c^2 \end{bmatrix} \begin{bmatrix} \epsilon_{11} \\ \epsilon_{22} \\ \epsilon_{12} \\ \alpha_{12} \\ \kappa_{31} \\ \kappa_{32} \end{bmatrix}, \quad (6)$$

which involves four independent elastic constitutive parameters: the Lamé constants λ and μ , the Cosserat shear modulus μ_c , and the so-called characteristic length l_c , which is responsible for the rotational stiffness.

The micropolar continuum adopted here is piecewise-homogeneous: it is a randomly structured two-phase composite made of matrix and disk-shaped inclusions. Both phases are linear elastic and isotropic while the mesoscale and macroscale models are linear elastic and generally anisotropic. These models are formulated as follows. We introduce a mesoscale window \mathcal{B}_δ of size L , and characterize it by a dimensionless mesoscale

$$\delta = \frac{L}{d}$$

where d is the inclusion size (Figure 2). The mesoscale stiffness properties of \mathcal{B}_δ are random and, generally, anisotropic. For spatially ergodic microstructures (such as assumed here) their scatter (or noise-to-signal) ratio decreases as δ increases, and one arrives at deterministic, macroscale properties of the RVE. In principle, lacking any spatial periodicity of the material, one has to take the limit $\delta \rightarrow \infty$, but, depending on the acceptable level of scatter, a finite mesoscale may be chosen (Ostoja-Starzewski, 2006).

The mesoscale properties are defined from generalized macrohomogeneity (Hill–Mandel type, (Hill, 1963; Mandel and Dantu, 1963)) conditions accounting for the presence of classical and micropolar variables (Li and Liu, 2009; Ostoja-Starzewski, 2011; Liu, 2013), here considered separately:

$$\frac{1}{V_\delta} \int_{\mathcal{B}_\delta} (\sigma_{ij} \epsilon_{ij} + \beta_{ij} \alpha_{ij} + \mu_{ij} \kappa_{ij}) dV = \bar{\sigma}_{ij} \bar{\epsilon}_{ij} + \bar{\beta}_{ij} \bar{\alpha}_{ij} + \bar{\mu}_{ij} \bar{\kappa}_{ij}, \quad (7)$$

where V_δ is the volume occupied by a material described above, while the overbars denote volume averaged quantities. In effect, Eq. (7) establishes an equivalence of the average internal work over \mathcal{B}_δ and the mechanical internal work density of the mesoscale model, expressed in terms of homogenized stress and strain measures.

Providing that the hyperelastic materials’ major symmetries hold, the general anisotropic 2D stress–strain relations, using the vectors defined in Eqs. (5), are written:

$$\begin{bmatrix} \bar{\sigma} \\ \bar{\beta} \\ \bar{\mu} \end{bmatrix} = \begin{bmatrix} \bar{\mathbb{A}} & \bar{\mathbb{D}} & \bar{\mathbb{F}} \\ \bar{\mathbb{D}}^T & \bar{\mathbb{B}} & \bar{\mathbb{G}} \\ \bar{\mathbb{F}}^T & \bar{\mathbb{G}}^T & \bar{\mathbb{C}} \end{bmatrix} \begin{bmatrix} \bar{\varepsilon} \\ \bar{\alpha} \\ \bar{\kappa} \end{bmatrix}, \quad (8)$$

or, in terms of components:

$$\begin{bmatrix} \bar{\sigma}_{11} \\ \bar{\sigma}_{22} \\ \bar{\sigma}_{12} \\ \bar{\beta}_{12} \\ \bar{\mu}_{31} \\ \bar{\mu}_{32} \end{bmatrix} = \begin{bmatrix} \bar{\mathbb{A}}_{1111} & \bar{\mathbb{A}}_{1122} & \bar{\mathbb{A}}_{1112} & \bar{\mathbb{D}}_{1112} & \bar{\mathbb{F}}_{1131} & \bar{\mathbb{F}}_{1132} \\ \bar{\mathbb{A}}_{2211} & \bar{\mathbb{A}}_{2222} & \bar{\mathbb{A}}_{2212} & \bar{\mathbb{D}}_{2212} & \bar{\mathbb{F}}_{2231} & \bar{\mathbb{F}}_{2232} \\ \bar{\mathbb{A}}_{1211} & \bar{\mathbb{A}}_{1222} & \bar{\mathbb{A}}_{1212} & \bar{\mathbb{D}}_{1212} & \bar{\mathbb{F}}_{1231} & \bar{\mathbb{F}}_{1232} \\ \bar{\mathbb{D}}_{1211} & \bar{\mathbb{D}}_{1222} & \bar{\mathbb{D}}_{1212} & \bar{\mathbb{B}}_{1212} & \bar{\mathbb{G}}_{1231} & \bar{\mathbb{G}}_{1232} \\ \bar{\mathbb{F}}_{3111} & \bar{\mathbb{F}}_{3122} & \bar{\mathbb{F}}_{3112} & \bar{\mathbb{G}}_{3112} & \bar{\mathbb{C}}_{3131} & \bar{\mathbb{C}}_{3132} \\ \bar{\mathbb{F}}_{3211} & \bar{\mathbb{F}}_{3222} & \bar{\mathbb{F}}_{3212} & \bar{\mathbb{G}}_{3212} & \bar{\mathbb{C}}_{3231} & \bar{\mathbb{C}}_{3232} \end{bmatrix} \begin{bmatrix} \bar{\varepsilon}_{11} \\ \bar{\varepsilon}_{22} \\ \bar{\varepsilon}_{12} \\ \bar{\alpha}_{12} \\ \bar{\kappa}_{31} \\ \bar{\kappa}_{32} \end{bmatrix}. \quad (9)$$

It is noticed that, in the case of centrosymmetric (i.e. non-chiral) materials, the components of tensors $\bar{\mathbb{D}}$, $\bar{\mathbb{F}}$ and $\bar{\mathbb{G}}$ are null. Henceforth, our strategy is to determine numerically, consistently with the macrohomogeneity condition (7), the components of the mesoscale stiffness tensors from a Dirichlet (D-BC) BVP. Separately, by solving the Neumann (N-BC) BVP, we will find the mesoscale compliance tensors. These conditions correspond to those proposed in (Onck, 2002).

- Dirichlet boundary conditions

We consider a square-shaped mesoscale domain \mathcal{B}_δ whose center is fixed at the origin of the coordinate system. On account of the above condition in Eq. (7), we set up the Dirichlet boundary conditions:

$$u_i = \bar{\varepsilon}_{ij}x_j, \quad \varphi_3 = \frac{1}{2}e_{ij3}\bar{\alpha}_{ij} + \bar{\kappa}_{3i}x_i \quad \text{on } \partial\mathcal{B}_\delta,$$

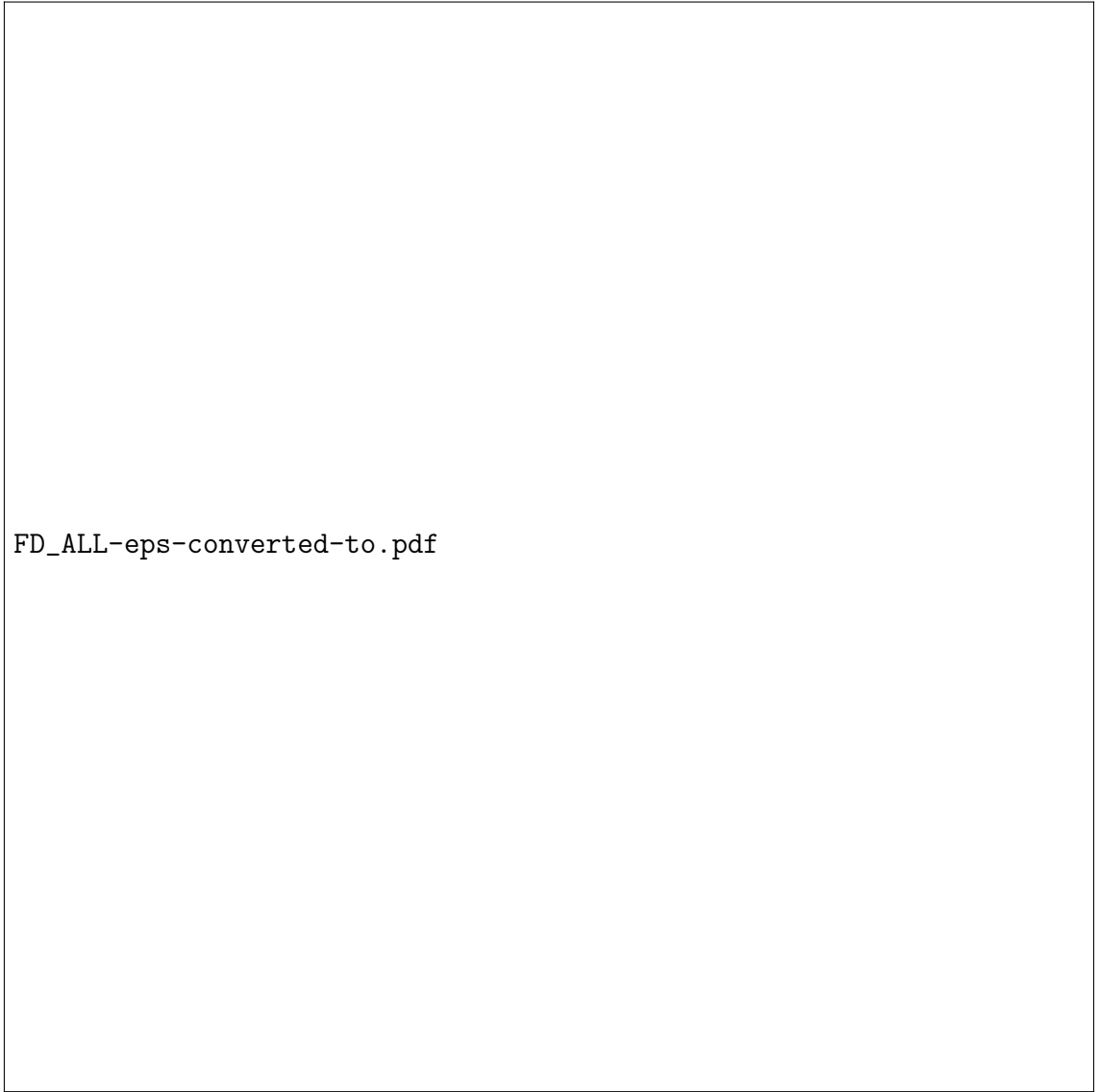
($i, j = 1, 2$). The strategy of applying the boundary conditions is outlined in Fig. 3. The solution of the cell problem under various combinations of boundary conditions yields the homogenized stresses ($i, j = 1, 2$):

$$\bar{\sigma}_{ij} = \frac{1}{V_\delta} \int_{\partial\mathcal{B}_\delta} (t_i x_j + t_j x_i) dA, \quad \bar{\beta}_{ij} = \frac{1}{2V_\delta} e_{ij3} \int_{\partial\mathcal{B}_\delta} m_3 dA, \quad \bar{\mu}_{3i} = \frac{1}{V_\delta} \int_{\partial\mathcal{B}_\delta} m_3 x_i dA.$$

- Neumann boundary conditions

In the case of Neumann boundary conditions, on account of Eq. (7), we impose (Fig. 4):

$$t_i = (\bar{\sigma}_{ij} + \bar{\beta}_{ij})n_j, \quad m_3 = m_3^o + \bar{\mu}_{3i}n_i \quad \text{on } \partial\mathcal{B}_\delta,$$



FD_ALL-eps-converted-to.pdf

Figure 3: Dirichlet boundary conditions (D-BC); deformed configurations and corresponding stresses in a homogeneous sample: classical (*i*) and micropolar modes (*ii*).

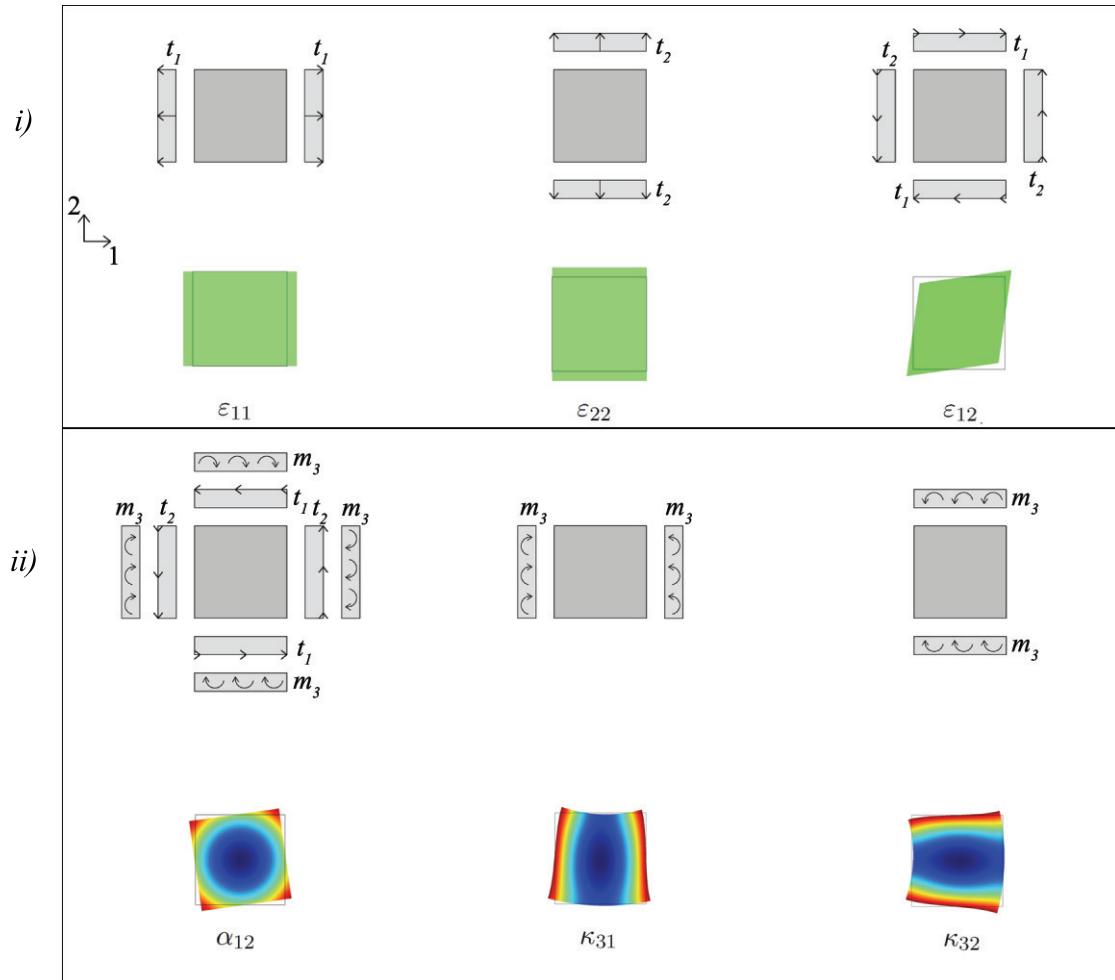


Figure 4: Neumann boundary conditions (N-BC); deformed configurations and corresponding strains in a homogeneous sample: classical (i) and micropolar (ii) surface tractions and couples.

where $m_3^o = - \int_{\partial\mathcal{B}} e_{ij3} x_i \bar{\beta}_{jk} n_k$ is the moment imposed to ensure the moment balance in the presence of skew-symmetric shear ($i, j, k = 1, 2$). The resulting homogenized strains are ($i, j = 1, 2$):

$$\bar{\varepsilon}_{ij} = \frac{1}{V_\delta} \int_{\mathcal{B}_\delta} \varepsilon_{ij} dV, \quad \bar{\alpha}_{ij} = \frac{1}{2V_\delta} \int_{\mathcal{B}_\delta} \alpha_{ij} dV, \quad \bar{\kappa}_{3i} = \frac{1}{V_\delta} \int_{\mathcal{B}_\delta} \kappa_{3i} dV.$$

The correct implementation of the boundary conditions described above has been tested on square-shaped mesoscale domains made of a homogeneous material.

3. Computer solutions of boundary value problems

3.1. Realizations of random two-phase composites

We study the scale-dependent effective response of a heterogeneous random material described as 2D and two-phase composites made of a base matrix with randomly distributed inclusions. In a composite material various parameters such as position, size, shape and density of inclusions as well as the mechanical properties of the constituent phases are spatially random. Here we fix the nominal volume fraction of the medium, the particles' shape (disk-shaped inclusions), the particles' size (diameter d) and the mechanical parameters of each phase.

With reference to Fig. 2, two material cases studied: (a) stiff inclusions in a soft matrix and (b) soft inclusions in a stiff matrix. The attention is here focused on the contrast between the Young's moduli of inclusions and matrix and the contrast between the so-called characteristic lengths between inclusions and matrix. The parameters of the two material cases are inverted. Without losing the generality of the statistical procedure developed to simulate the realizations of such composites with spatial randomness, case (a) can be referred to concrete masonry and case (b) to filled rubble masonry or magmatic rock structures.

The constitutive response of a non-periodic heterogeneous material requires the definition of the size of a RVE, L_{RVE} , larger than the microscale characteristic length, d , so that to render the influence of the boundary conditions on the RVE to vanish. This prescription ensures a homogenization limit in the sense of Hill but generically states that $L_{RVE} \gg d$, for instance that L_{RVE} is about 10 up to 100 times larger than the heterogeneity size (Ostoja-Starzewski, 2006; Khisaeva and Ostoja-Starzewski, 2006). According to the approach presented in the above mentioned papers, as well as in (Du and Ostoja-Starzewski, 2006) and (Ostoja-Starzewski, 2008), in this section we present a procedure which requires the statistical definition of a number of realizations of the possible microstructure, sampled in a Monte-Carlo sense, which allows us the determination of statistics of scale-dependent upper and lower bounds for the overall elastic moduli approaching the RVE size.

In particular, we identify finite size test windows as portions of the heterogeneous material (SVEs) on which we perform homogenization by solving both Dirichlet and Neumann

classical and micropolar BVPs, separately as defined in Sec. 2. The realizations of the microstructure, that is, the number and position of inclusions within any window, are generated by a hard-core Poisson point field (i.e. not allowing for disks' overlaps), thus simulating a mesoscale window placed anywhere in the random medium. By increasing the window size and exploiting the results in terms of the statistical convergence of the average results of the Dirichlet and Neumann BVPs, respectively, we then obtain the RVE size and estimate the corresponding effective elastic coefficients.

Let the random medium be a set $B = \{B(\omega); \omega \in \Omega\}$ of realizations $B(\omega)$ defined over a sample space Ω , ω being an elementary event. Under the hypothesis of statistical homogeneity and isotropy combined with the mean-ergodicity of the medium, we generate particle distributions by a hard-core Poisson point field. The entire computational stochastic mechanics procedure is structured as follows (Fig. 5).

1. Set a nominal area fraction ρ , defined as the ratio between the total area of the inclusions and the area of a test window. Select a window size L and define the dimensionless scale factor $\delta = \frac{L}{a}$.
2. For each mesoscale window (δ): determine the number of disks via simulations of the Poisson random variable (Knuth's algorithm), where the Poisson's distribution is characterized by the parameter $p_\delta = (\rho L^2)/[\pi(d/2 + s/2)^2]$, with s being the minimum distance between disk boundaries ('hard-core' interactions) fixed in order to avoid very narrow necks between the inclusions. Here ρ (fixed at 40%) is the nominal areal fraction of inclusions.
3. Then simulate (uniform) random dispositions of disks' centres, that is the realizations $\mathcal{B}_\delta(\omega)$ of portions of the random medium. Each realization is independent from any previous one.
4. For each $\mathcal{B}_\delta(\omega)$, solve both the Dirichlet and the Neumann BVP defined in Sec. 2 and obtain the relative homogenized constitutive parameters.
5. Repeat steps 2–4 until the confidence interval of the average homogenized constitutive parameters set at 95%, evaluated over a normal standard distribution, is less than a small desired value, which depends on the data dispersion (as illustrated in Subsection 3.2).
6. If the number of realizations necessary for ensuring the requirement in step 5 is small enough (also depending on the data dispersion, as illustrated in Subsection 3.2), stop the procedure. Otherwise choose an increased value of δ and go to step 2.

On account of the spatial homogeneity of the Poisson point process, the steps 2–5 correspond to moving the window anywhere within a material domain (Fig. 6), thereby accounting for the presence of inclusions that intersect the window's edges.

The fulfillment of the requirement at step (6) means that the values of the homogenized constitutive coefficients are distributed around their averages with a vanishing variation coefficient and that the RVE size is achieved. The effective constitutive moduli are finally estimated as the mean values between the Dirichlet (upper) and Neumann (lower) bounds at the convergence window (RVE).

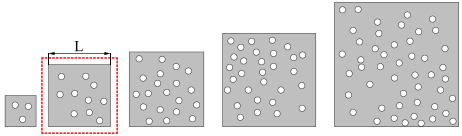
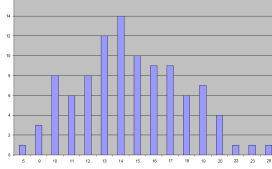
<p>1. SETTING THE PARAMETERS</p> <p>▷ ρ: nominal volume fraction of the medium</p> <p>▷ d: diameter of the inclusions</p> <p>▷ s: ‘hard-core’ distance</p> <p>▷ L: window size</p> <p>▷ $\delta = \frac{L}{d}$: scale parameter</p> <p><code>density-eps-converted-to.pdf</code></p> 	
<p>2. DETERMINE THE EXPECTED NUMBER OF INCLUSIONS in each trial window of size δ</p> <p>▷ Poisson’s distribution parameter: $p_\delta = \rho L^2 / \pi(d/2 + s/2)^2$</p> 	
<p>3. GENERATE REALIZATIONS $\mathcal{B}_\delta(\omega)$ of the disordered medium</p> <p><code>different_win-eps-converted-to.pdf</code></p>	<p>4. SOLVE DIRICHLET AND NEUMANN BVP for each $\mathcal{B}_\delta(\omega)$</p> <p><code>bound-eps-converted-to.pdf</code></p>
<p>5. REPEAT STEPS 2-4 until reaching the desired statistical accuracy for windows of increasing size δ</p> <p><code>increasing_win-eps-converted-to.pdf</code></p>	<p>6. REACH THE CONVERGENCE (RVE SIZE, ELASTIC MODULI)</p> <p><code>convergence-eps-converted-to.pdf</code></p>

Figure 5: Schematic of the performed statistical procedure.

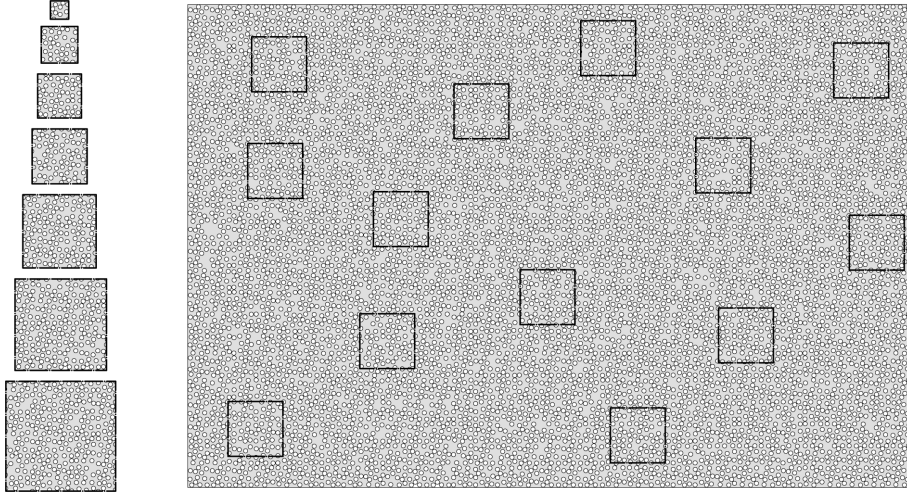


Figure 6: Different $\mathcal{B}_\delta(\omega)$ within a portion of a random medium.

Note that the statistical criterion adopted allows us to detect the RVE size also when the Dirichlet and Neumann solution do not tend to the same value. Indeed, the mismatch between the two solutions, which depends on the material contrast (Ostoja-Starzewski, 2006) as rigorously illustrated in terms of stretched–exponential scaling functions in (Ranganathan and Ostoja–Starzewski, 2009), can be such as to affect the validity of a scale–dependent homogenization via hierarchies of bounds (Salmi et al., 2012). On this basis, in Subsection 3.2 the RVE size for both materials with high (a) and low (b) contrasts, the latter with bounds significantly different, are estimated.

3.2. Numerical simulations

In order to investigate the response of the two paradigmatic material cases of Fig. (2), we adopt the procedure described in Sec. 3.1 with the nominal area fraction in both cases being $\rho = 40\%$, the diameter d of inclusions set at 10 mm , the hard-core distance $s = 1\text{ mm}$, and taking window sizes at δ from 5 through 25. The analyses are confined to the 2D elastic framework. The adopted material parameters: Young’s modulus, E , Poisson’s coefficient, ν , micropolar shear modulus, μ_c , and characteristic length, l_c , are reported in Table 1. It is also assumed that the Cosserat shear modulus takes the same value as the classical shear modulus.

For each finite–size test window, the Dirichlet BVPs defined in Sec. 2 are numerically solved using the code COMSOL Multiphysics $\text{\textcircled{R}}$. and all the homogenized constitutive parameters of Eq. (9) are evaluated. Similarly, the Neumann BVPs are solved to determine the homogenized compliances according to a relation inverse to Eq. (9). This code is based on a finite element method in which it is possible to directly implement, both in weak or strong form, the equations governing the problem to investigate; this is especially suitable for solving non–classical BVPs. In particular, we adopted unstructured meshes of triangular quadratic Lagrangian finite elements and paid special attention to solve the

Material		Parameters			
		E [MPa]	ν	μ_c [MPa]	l_c [mm]
a	matrix	5000	0.15	2710	0.1
	inclusions	30000	0.4	10700	1
b	matrix	30000	0.4	10700	1
	inclusions	5000	0.15	2710	0.1

Table 1: Material parameters.

BVPs in the presence of non-homogeneous boundary, developing automatic procedures for dealing with a very large number of material realizations $\mathcal{B}_\delta(\omega)$.

In Eqs. (8, 9) the most general form of the linear elastic constitutive law for the 2D anisotropic Cosserat medium is reported. Nevertheless, for the materials here accounted for, the resulting homogenized mesoscale components of the tensors $\overline{\mathbb{D}}$, $\overline{\mathbb{F}}$ and $\overline{\mathbb{G}}$ are always equal to zero (central symmetry). We have separately studied the components of the classical tensors $\overline{\mathbb{A}}$ and of the micropolar tensors $\overline{\mathbb{C}}$ and $\overline{\mathbb{B}}$. In particular, the longitudinal elastic coefficients being predominant, we focused the attention on the scalar terms of stiffnesses of the equivalent anisotropic continuum: $\overline{\mathbb{A}} = (\overline{\mathbb{A}}_{1111} + \overline{\mathbb{A}}_{2222})/2$, classical, and $\overline{\mathbb{B}}_{1212}$, $tr\overline{\mathbb{C}}$, micropolar.

The results in terms of convergence trend of the ensemble average homogenized stiffness coefficients are presented and commented on below. For all the cases analyzed, the RVE size δ_{RVE} was judged as attained, when the statistical accuracy of 95% relative to a standard normal distribution was attained.

Figs. 7 and 8 report, for the material cases (a) and (b), the average values of classical and micropolar stiffness measures, $\langle \overline{\mathbb{A}} \rangle$ and $\langle tr\overline{\mathbb{C}} \rangle$, normalized with respect to the average value of the same measures estimated at the convergence window, $\langle \overline{\mathbb{A}}_{RVE} \rangle$ and $\langle tr\overline{\mathbb{C}}_{RVE} \rangle$, versus the number of simulations performed for different widow sizes. The reported values correspond to solutions of Dirichlet boundary problems for any $\mathcal{B}_\delta(\omega)$ allowing inclusions to randomly intersect the boundary $\partial\mathcal{B}_\delta(\omega)$. These figures provide a picture of the statistical convergence criterion adopted to stop the simulation for any given window size.

With reference to the procedure of Sec. 3.1 (step 5), the number of realizations N for each test window has been chosen such that $\frac{1.96}{\langle X_{\overline{\delta}} \rangle} \frac{\sigma}{\sqrt{N}} \leq tol$, where σ is the standard deviation, $\langle X_{\overline{\delta}} \rangle$ is the average stiffness estimated at a given $\delta = \overline{\delta}$ and tol is a given tolerance set equal to 0.005 for the material (a) and equal to 0.0025 for the material (b), which shows less dispersion. It can be observed that, by increasing the scale factor δ , the confidence interval is reached and the average stiffness values converge after a more and more reduced number of realizations $\mathcal{B}_\delta(\omega)$. The RVE size (δ_{RVE}) and the corresponding

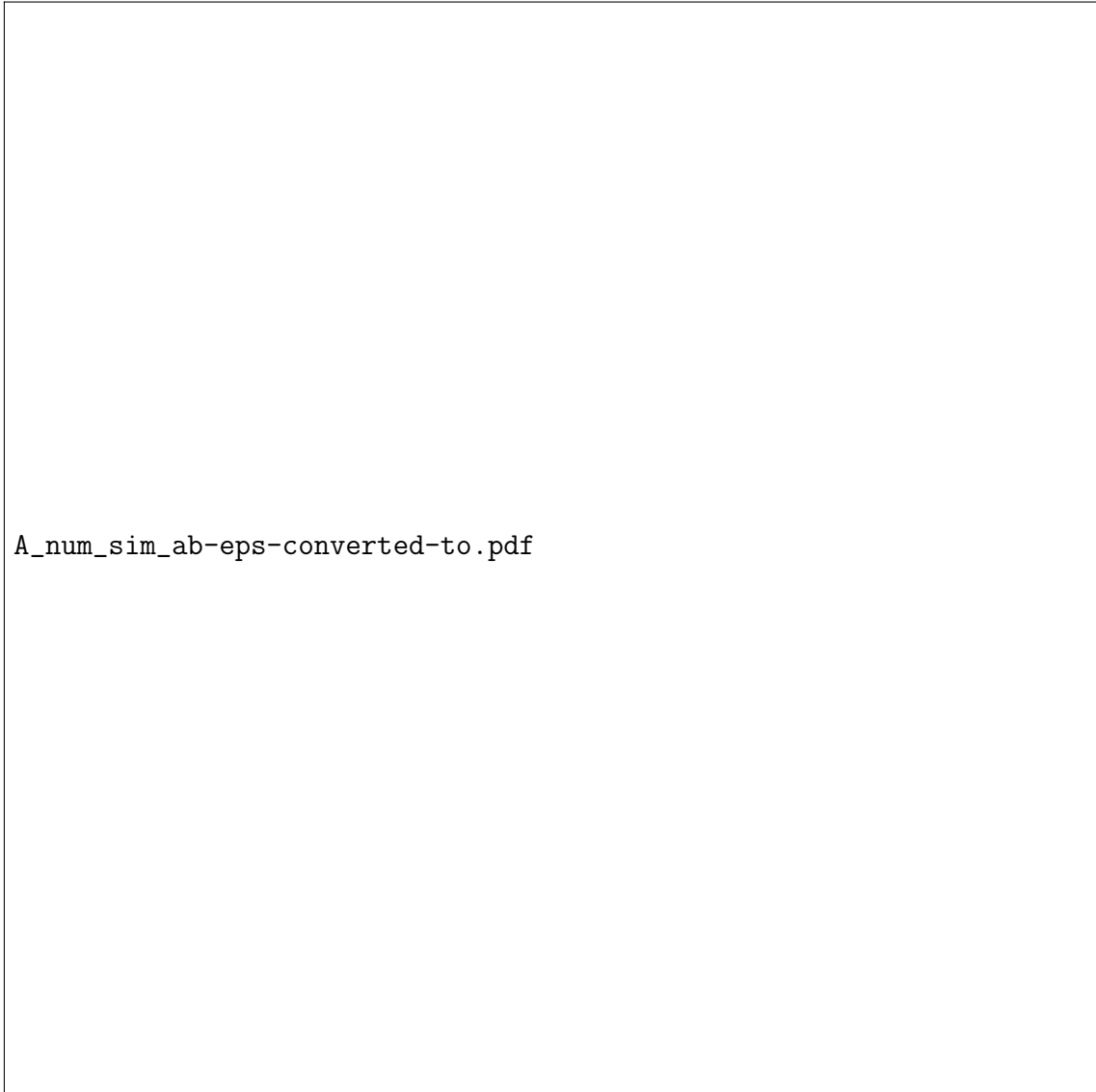


Figure 7: Average values of \bar{A} (normalized to $\langle \bar{A}_{RVE} \rangle$; Dirichlet solutions) versus the number of simulations performed for different window sizes (δ). Material (a), left side; material (b), right side.

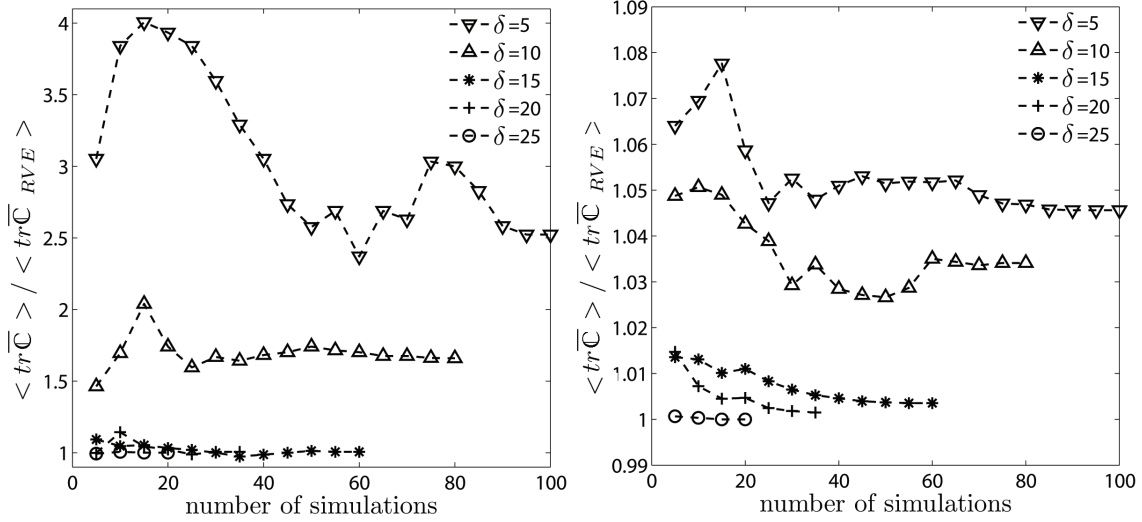


Figure 8: Average values of $tr\bar{\mathbb{C}}$ (normalized to $\langle tr\bar{\mathbb{C}}_{RVE} \rangle$; Dirichlet solutions) versus the number of simulations performed for different window sizes (δ). Material (a), left side; material (b), right side.

average values of the effective constitutive parameters are then attained without dispersion at the minimum window size for which the number of necessary realizations N is less than a small number (i.e. 5; step 6). This circumstance also corresponds to reaching the minimum window size (δ_{RVE}) for which the estimated homogenized moduli remain constant, within a tolerance interval less than 0.5%, for both the Dirichlet and Neumann solutions. Thus, as observed above, the statistical convergence criterion adopted allows us to determine the scale δ_{RVE} also in the presence of discrepancies between upper and lower bounds, which can be significant for weak levels of material contrast (Ostoja-Starzewski, 2006), so as to induce the search for solutions alternative to the upper–lower bounding solutions (Salmi et al., 2012).

The decrease of statistical dispersion with the increase of the mesoscale δ is also shown in Fig.9, where the Coefficients of Variation (defined as the ratio of the standard deviation to the mean: $CV = \sigma / \langle X_{\bar{\delta}} \rangle$) of the average values of $\bar{\mathbb{A}}$ and $tr\bar{\mathbb{C}}$ obtained for materials (a) and (b) are reported.

As expected, the scatter reduces, in both media, by increasing the window size and it is always slightly greater in the medium with higher contrast (a).

As described in Sec. 3.1, the SVE ideally corresponds to a portion of the actual random medium $\mathcal{B}_{\delta}(\omega)$ in which inclusions are not prevented from intersecting the window edges. Thus, the numerical simulations are performed by taking into account non-homogeneous boundaries $\partial\mathcal{B}_{\delta}(\omega)$ (crossing-inclusions). We also consider the less realistic case, widely used in literature, of homogeneous boundaries in which inclusions do not intersect the windows' edges (non-crossing inclusions). The comparison between the homogenized responses obtained by performing numerical simulations for the two cases, either applying Dirichlet and Neumann boundary conditions, allows us to emphasize the influence of

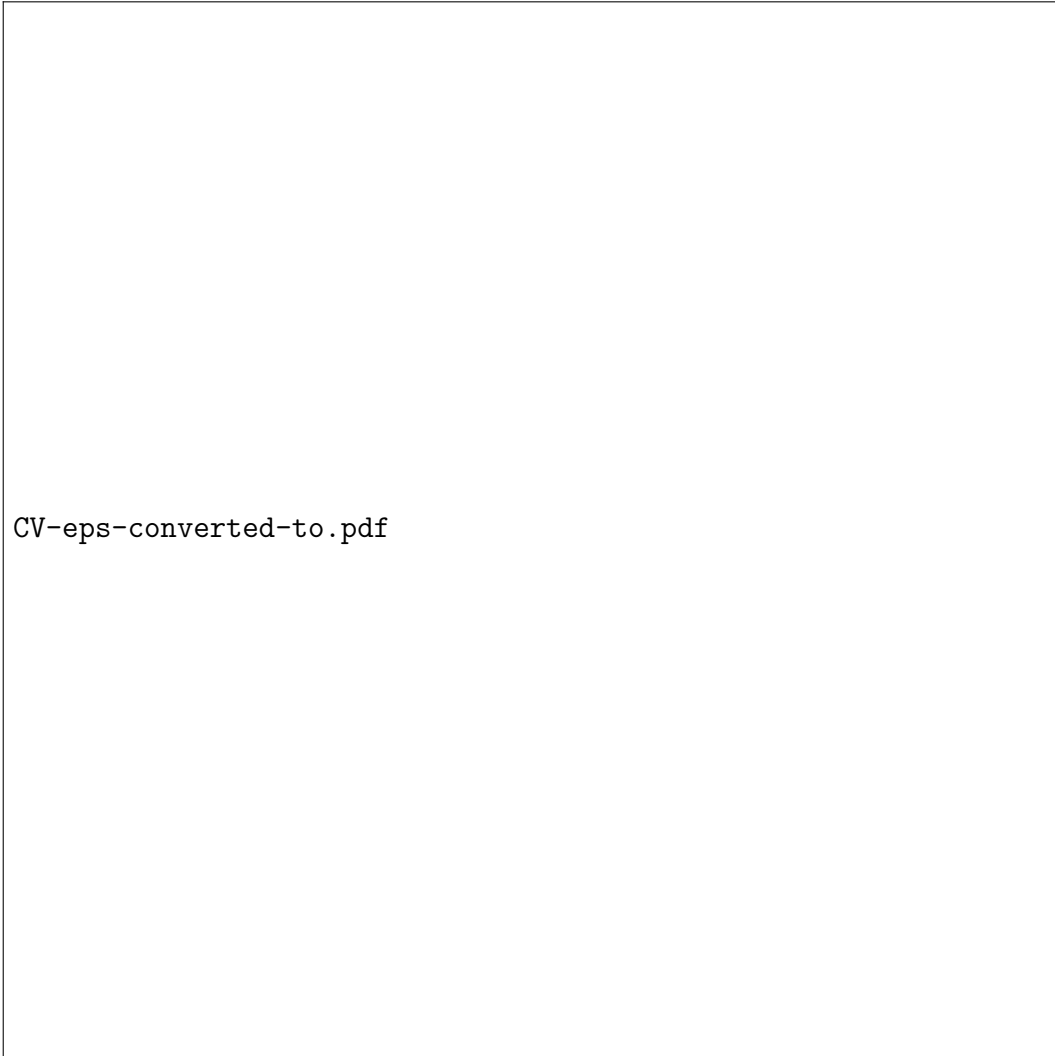


Figure 9: Coefficient of Variation (CV) of $\langle \bar{A} \rangle$ (left) and $\langle tr\bar{C} \rangle$ (right) for various δ .

positions of the inclusions with respect to the SVE's boundary, as is shown in the following.

Fig. 10 reports the average of the classical stiffness coefficient $\bar{\mathbb{A}}$ versus the scale parameter δ , obtained by solving the Dirichlet and Neumann BVPs for both materials (a) and (b). It can be noticed that the convergence trend is different in the case of inclusions that cross or do not cross the SVEs boundary. In particular, for the higher contrast material (a) $\delta_{RVE} = 20$ in the case of crossing inclusions, while $\delta_{RVE} = 25$ in the case of non-crossing inclusions. In the presence of stiff inclusions which randomly intersect the SVE boundary, we get an average stiffness value between Dirichlet and Neumann solution higher by 8.22% than the corresponding value obtained for inclusions prevented from intersecting the boundary. The lower contrast material (b) shows a slower convergence trend. Accordingly, the RVE is attained for $\delta_{RVE} = 25$ in the case of crossing inclusions, while in the case of non-crossing inclusions $\delta_{RVE} > 25$. The convergence value of the average stiffness in the presence of soft inclusions that intersect the RVE boundary is lower by 3.4% than in the case of non-crossing inclusions.

Overall, these results confirm the influence on the gross material response of the variation of the position of the test window, and this influence is more appreciable for the higher contrast material (a).

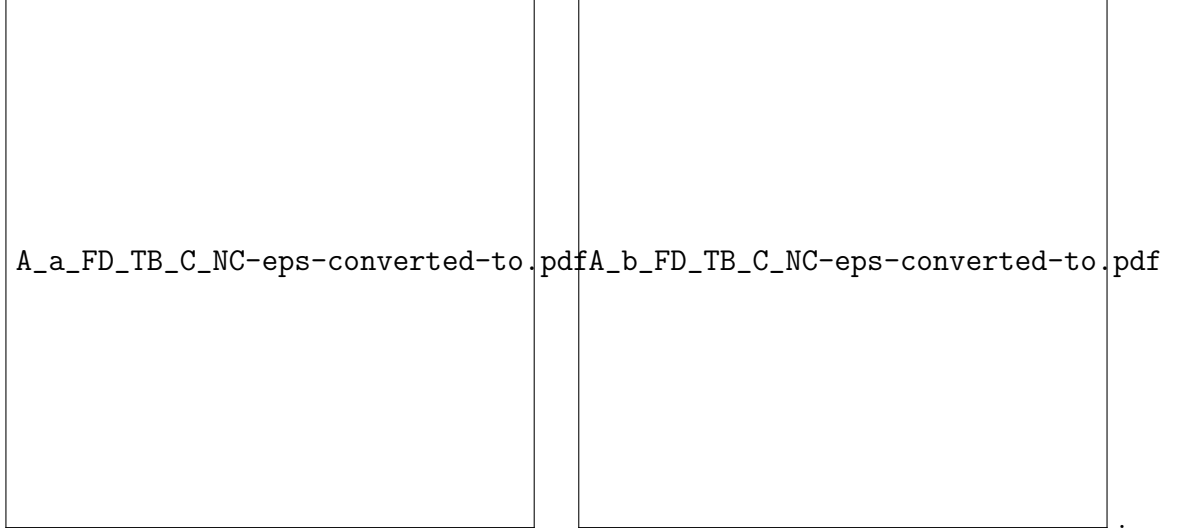


Figure 10: Hierarchy of scale dependent effective constitutive parameters: $\langle \bar{\mathbb{A}} \rangle$ obtained for higher (a; left side) and lower (b; right side) material contrasts. Dirichlet (D-BC) and Neumann (N-BC) BVPs solutions obtained with inclusions crossing (dash lines) and non-crossing (solid lines) $\partial\mathcal{B}_\delta(\omega)$.

Fig. 11 reports the average homogenized values $\langle \bar{\mathbb{B}}_{1212} \rangle$ versus the mesoscale δ . Materials (a) and (b) exhibit convergence trends similar to the coefficient $\bar{\mathbb{A}}$, highlighting that also for the skew-symmetric strain-stress behaviour analogous differences arise between the two considered composite materials. In particular, in the random case of inclusions that intersect the RVE boundary, the material (a) is stiffer by 3.3%, whereas the material (b) softer of 1.5% relative to the case of inclusions embedded entirely within

the window. The convergence values for RVE sizes coincide with the corresponding values obtained for the classical term $\overline{\mathbb{A}}$.

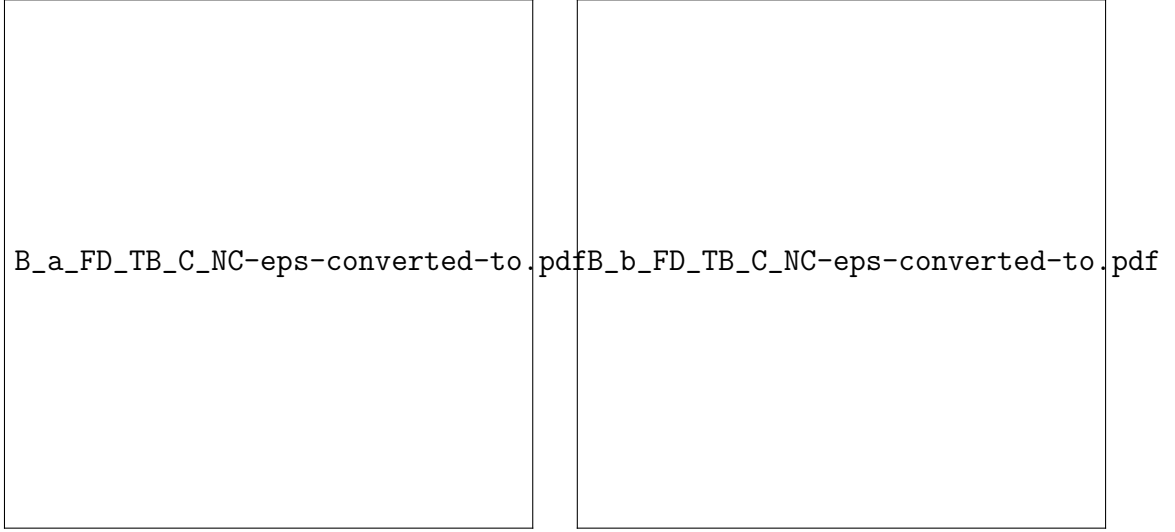


Figure 11: Hierarchy of scale dependent effective constitutive parameters: $\langle \overline{\mathbb{B}}_{1212} \rangle$ obtained for higher (a; left side) and lower (b; right side) material contrasts. Dirichlet(D-BC) and Neumann (N-BC) BVPs solutions obtained with inclusions crossing (dash lines) and non-crossing (solid lines) $\partial\mathcal{B}_\delta(\omega)$.

Fig. 12 shows the micropolar results in terms of the average homogenized characteristic length parameter $\langle \bar{l}_c \rangle = \langle \sqrt{\text{tr}(\overline{\mathbb{C}})/\overline{\mathbb{B}}_{1212}} \rangle$. The material (a) still exhibits differences between the curves obtained in the cases of crossing and non-crossing inclusions, but in the case of lower contrast material (b) such differences are more predominant. For the higher contrast material (a), the RVE is attained at $\delta_{RVE} = 15$ in the case of crossing inclusions and at $\delta_{RVE} = 20$ in the case of non-crossing inclusions. In the presence of stiff inclusions that intersect the RVE boundary we find an average stiffness value between Dirichlet and Neumann solution 35% greater than for the case of inclusions embedded in the window. This is also the case for the low contrast material. The estimated micropolar average stiffness value is smaller than 20% relative to the case of a homogeneous boundary.

Considering these results, it emerges that in both materials (a) and (b), the variation of the test window position in the medium (i.e. variation of the position of the inclusions in the window $\mathcal{B}_\delta(\omega)$) has an influence on the gross material response greater than that appreciated in the classical case. This aspect is apparent in particular in case (a). This is also due to the higher differences between the micropolar moduli of the two phases rather than between the classical moduli.

It can be also noticed that in the material (b), due to the lower contrast of the composite, the mismatch in the values of $\langle \bar{l}_c \rangle$, obtained as solutions of Dirichlet and Neumann BVPs in the case of crossing-inclusions, is greater than in the material (a). In both cases, the average values between the two solutions tend to the value of the characteristic length of the matrix l_c . It is therefore noticeable that Cosserat bending effects are weaker when

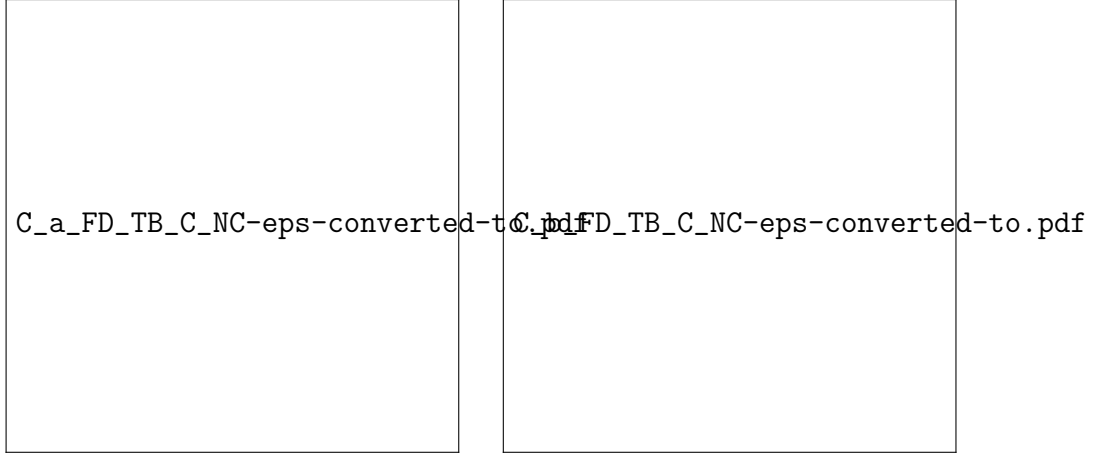


Figure 12: Hierarchy of scale dependent effective constitutive parameters: $\langle \bar{l}_c \rangle = \langle \sqrt{\text{tr}(\bar{\mathbb{C}})/\bar{\mathbb{B}}_{1212}} \rangle$ obtained for higher (a; left side) and lower (b; right side) material contrasts. Dirichlet (D-BC) and Neumann (N-BC) BVPs solutions obtained with inclusions crossing (dash lines) and non-crossing (solid lines) $\partial\mathcal{B}_\delta(\omega)$.

the medium has higher contrast (a), but are stronger in the case of lower contrast (b). These findings are in agreement with some experimental results (Gauthier, 1982; Lakes, 1983, 1986, 1995). In Lakes (1986) for instance, the author focused on two different porous solids: a polyurethane foam characterized by rigid matrix and soft inclusions and a syntactic foam with soft matrix and rigid inclusions, and concluded that Cosserat effects are found only in the latter case. However, it is also worth noting that the homogenized values of the micropolar elastic shear tensor $\bar{\mathbb{B}}$ are not negligible in any case considered here. These effects have not yet been investigated experimentally. Then, although the characteristic effective length converges to very low values for the material (a), the micropolar continuum still provides additional information (i.e. relative rotation, measure of the non-symmetry of strain). As widely shown in the case of anisotropic periodic materials (Pau and Trovalusci, 2011; Trovalusci and Pau, 2014).

4. Discussion of results and final comments

This work studies scale-dependent micropolar homogenization of random micropolar materials, our motivation coming from composite materials such as ancient masonry. Attention is focused on particle composites, made of random distribution of inclusions in a matrix, with two cases: (a) stiff inclusions embedded in a soft matrix, and (b) soft inclusions in a stiff matrix. The homogenization procedure specifically developed to deal with non-periodic composites has been developed based on hierarchies of solutions to Dirichlet and Neumann boundary value problems (BVPs), defined on 2D two-phase linear elastic continua of Cosserat type. This procedure employs a statistical process based on the assumptions of mean ergodicity and statistical homogeneity of the medium. The

statistical approach proposed follows the conceptual lines described in (Ostoja-Starzewski, 2006; Du and Ostoja-Starzewski, 2006), with reference to classical materials, and has been developed to account for the presence of both classical and micropolar field descriptors, separately. For each mesoscale test window the number and placement of inclusions vary according to a hard-core Poisson point process of disks' centres, thus simulating a window moving within a random domain, the SVE. The RVE at which we evaluate the effective elastic classical and non-classical moduli is approached approximately by increasing the size of SVE until reaching the desired statistical accuracy with a minimum number of simulations. It is worth noting that the adopted statistical convergence criterion allows attainment of the RVE even for materials with strong contrast in moduli Ostoja-Starzewski (2006). Notably, in both material cases studied – stiff inclusions in a soft matrix (case a) and the reverse (case b) – the RVE size for the bending micropolar moduli is smaller than that obtained for the classical moduli. Furthermore, the RVE is attained at larger window sizes when a special condition is introduced preventing the inclusions from crossing the window boundary.

On the other hand, for such materials with the given volume fraction (40%), the higher contrast medium (a) shows, with respect to the lower contrast medium (b), a slightly higher dispersion, of the averages of the effective elastic coefficients, to the variation of the number and the position of inclusions within the mesoscale windows; that is to the variation of the position of the test window in the random medium. Nevertheless in both cases, the scatter of results quickly falls as the window size increases. At the convergence window, the variation coefficient of the average coefficients varies within a range of 0.01 – 0.1%.

More comments are in place concerning the special random model in which inclusions are prevented from intersecting the window boundaries. In general, we find that the higher contrast medium (a) is slightly more sensitive than the medium (b) to the presence of inclusions which cross the windows' edges. In particular, the medium (a) when the stiff inclusions cross the boundary is stiffer than in the case in which inclusions are forced not to cross the boundary; conversely, the medium (b) with soft crossing inclusions is softer with respect to the case of non-crossing inclusions. Moreover, the differences in terms of average effective moduli and RVE sizes achieved, in the presence of crossing or non-crossing inclusions, reduce but remain when the window size increases. These differences are more appreciable when the micropolar moduli are evaluated; this is also because the differences between the micropolar bending moduli of the material phases (characteristic lengths), in both cases (a) and (b), are higher than the differences between the classical (Young's) moduli.

Overall, the statistical simulations show that it is not correct, both in the classical and the micropolar case, to neglect the presence of inclusions that intersect the windows' edges. The less realistic case, widely used in literature, in which the inclusions are prevented from crossing the windows' edges (thereby violating the hypothesis of statistical uniformity) provides results significantly different compared to the results obtained taking into account inclusions intersecting the windows' edges; this also occurs when the

test windows are sufficiently large. This finding has been confirmed by a study which also considers the the scale-dependent response of random media under periodic boundary conditions, for both displacements and rotations (Trovalusci et al., 2014). In order to lower the computational burden, it will be useful to verify, in future developments, whether a homogenization procedure approaching the RVE via finite-size windows (with the same convergence criterion as adopted here) considering specifically conceived periodized boundary conditions (Sab and Nedjar, 2005; Gitman et al., 2007) can be performed without resorting to scale-dependent lower (Neumann) and upper (Dirichlet) bounds. To some extent, these questions are addressed in detail in an ongoing work, where a statistical study, obtained by varying the size and position of the window, is performed based on the solution of BVPs with centro-symmetric crossing-inclusions and periodic boundary conditions.

Finally, it is observed, in agreement with experimental work (Lakes, 1983), that in the material (a) with higher contrast between the characteristic lengths of the material phases (inclusions/matrix), the curvature effects are less significant than in the case of material with low contrast (b). Nevertheless, the elastic modulus relating the relative rotation, which measures the skew-symmetric part of the strain, to the skew-symmetric part of the shear stress, does not vanish as the window size increases. This implies that in the presence of significant non-symmetric strain and shear effects, occurring in strongly anisotropic materials, the Cosserat description is more appropriate; like in the widely investigated case of anisotropic periodic materials (Pau and Trovalusci, 2011; Trovalusci and Pau, 2014). Further confirmations of the suitability of a micropolar model are expected from a more complete, ongoing analysis that considers not only the randomness of the positions but also the orientation of the inclusions of shape other than circular.

5. Acknowledgments

This research has been partially supported by the Italian ‘Ministero dell’Università e della Ricerca Scientifica’ (Research grant MIUR:Prin 2010-11) and by the NSF under grant CMMI-1030940. The authors wish to thank Dr. Stefano Marcelli (Department of Market and Payment System Oversight, Bank of Italy) for the methodological support in developing the statistical procedures and for the implementation of the relating software.

References

- Addessi, D., Sacco, E., 2012. A multi-scale enriched model for the analysis of masonry panels. *Int J Solids Struct* 49 (6), 865–880.
- Anthoine, A., 1995. Derivation of the in-plane elastic characteristics of masonry through homogenization theory. *Int J Solids Struct* 32 (2), 137–163.
- Bacigalupo, A., Gambarotta, L., 2011. Non-local computational homogenization of periodic masonry. *Int J Multiscale Com* 9 (5), 565–578.

- Capriz, G., 1989. *Continua with Microstructure*. Springer-Verlag, Berlin.
- Cavalagli, N., Cluni, F., Gusella, V., Mar. 2011. Strength domain of non-periodic masonry by homogenization in generalized plane state. *Eur J Mech A–Solid* 30, 113–126.
- Cecchi, A., Sab, K., 2009. Discrete and continuous models for in plane loaded random elastic brickwork. *Eur J Mech A–Solid* 28, 610–625.
- De Bellis, M. L., Addessi, D., 2011. A Cosserat based multi-scale model for masonry structures. *Int J Multiscale Com* 9 (5), 543–563.
- Du, X., Ostoja-Starzewski, M., 2006. On the scaling from statistical to representative volume element in thermoelasticity of random materials. *Netw Heterog Media* 1, 259–274.
- Eringen, A. C., 1999. *Microcontinuum Field Theories*. Springer-Verlag, New York.
- Forest, S., Dendievel, R., Canova, G., 1999. Estimating the overall properties of heterogeneous Cosserat materials. *Modelling Simul Mater Sci Eng* 7, 829–840.
- Forest, S., Pradel, F., Sab, K., 2001. Asymptotic analysis of heterogeneous Cosserat media, *Int J Solids Struct* 38, 4585–4608.
- Gauthier, R. D., 1982. Experimental investigation on micropolar media. In: Brulin, O., Hsies, R. K. T. (Eds.), *Mechanics of micropolar media*. Word Scientific, Singapore, pp. 395–463.
- Ghosh, S., 2011. *Micromechanical Analysis and Multi-scale Modeling using the Voronoi Cell Finite Element Method*. CRC Press, Taylor & Francis, Boca Raton (FL).
- Gitman, I. M., Askes, H., Sluys, L. J., 2007. Representative volume: existence and size determination. *Eng Fract Mech* 74, 2518–2534.
- Gusella, V., Cluni, F., 2006. Random field and homogenization for masonry with nonperiodic microstructure. *J Mech Mater Struct* 11 (1), 357–386.
- Hatami–Marbini, H., Picu, R. C., 2009. Heterogeneous long-range correlated deformation of semiflexible random fiber networks. *Phys Rev Lett E* 80, 046703-1–046703-11.
- Hill, R., 1963. Elastic properties of reinforced solids: some theoretical principles. *J Mech Phys Solids* 11, 357–372.
- Kanit, T., Forest, S., Galliet, I., Mounoury, V., Jeulin, D., 2003. Determination of the size of the representative volume element for random composites: statistical and numerical approach. *Int J Solids Struct* 40, 3647–3679.

- Khisaeva, Z., Ostoja-Starzewski, M., 2006. On the size of rve in finite elasticity of random composites. *J Elasticity* 85, 153–173.
- Kouznetsova, V. G., Geers, M. G. D., Brekelmans, W. A. M., 2002. Multi-scale constitutive modelling of heterogeneous materials with a gradient-enhanced computational homogenization scheme. *Int J Numer Meth Eng* 54, 1235–1260.
- Kouznetsova, V. G., Geers, M. G. D., Brekelmans, W. A. M., 2004. Multi-scale second-order computational homogenization of multi-phase materials: a nested finite element solution strategy. *Comput Method Appl M* 193 (48), 5525–5550.
- Lakes, R. S., 1983. Size effects and micromechanics of a porous solid. *J Mater Sci* 18, 2752–2581.
- Lakes, R. S., 1986. Experimental microelasticity of two porous solids. *Int J Solids Struct* 22 (1), 55–63.
- Lakes, R. S., 1995. Experimental methods for study of Cosserat elastic solids and other generalized elastic continua. In: Mühlhaus, H. B. (Ed.), *Continuum Models for Materials with Microstructure*. Wiley, New York, pp. 1–22.
- Li, X., Liu, Q., 2009. A version of Hill’s lemma for Cosserat continuum. *Acta Mech Sinica* 25, 499–506.
- Liu, Q., 2013. Hill’s lemma for the average–field theory of Cosserat continuum. *Acta Mech* 224, 851–866.
- Luciano, R., Sacco, E., 1997. Homogenization technique and damage model for old masonry material. *Int J Solids Struct* 34, 3191–3208.
- Mandel, J., Dantu, P., 1963. Contribution à l’étude théorique et expérimentale du coefficient d’élasticité d’un milieu hétérogènes mais statistiquement homogène. *Annales des Ponts et Chaussées Paris* 6, 115–145.
- Milani, G., Lourenço, P. B., 2010. Monte Carlo homogenized limit analysis model for randomly assembled blocks in-plane loaded. *Comput Mech* 46 (6), 827–849.
- Nowacki, W., 1970. *Theory of Micropolar Elasticity*. Springer Verlag, Wien, New York, CISM Lectures Notes.
- Nowacki, W., 1986. *Theory of Asymmetric Elasticity*. Pergamon Press, Oxford.
- Onck, P. R., 2002. Cosserat modeling of cellular solids. *CR Mécanique* 330, 717–722.
- Ortiz, M., Phillips, R., 1999. Nanomechanics of defect in solids. In: Van der Giessen, E., Wu, T. (Eds.), *Advances in Applied Mechanics*. Vol. A36. Academic Press, San Diego, pp. 1–73.

- Ostoja–Starzewski, M., Du, X., Khisaeva, Z., Li, W., 2007. Comparisons of the size of representative volume element in elastic, plastic, thermoelastic, and permeable random microstructures. *Int J Multiscale Com* 5, 73–82.
- Ostoja–Starzewski, M., 2011. Macrohomogeneity condition in dynamics of micropolar media. *Arch Appl Mech* 81, 899–906.
- Ostoja–Starzewski, M., 2008. *Microstructural Randomness and Scaling in Mechanics of Materials*, Modern Mechanics and Mathematics Series. Chapman & Hall/CRC/Taylor & Francis.
- Ostoja–Starzewski, M., 2006. Material spatial randomness: from statistical to representative volume element. *Probabilist Eng Mech* 21, 112–132.
- Ostoja–Starzewski, M., 1998. Random field models of heterogeneous materials. *Int J Solids Struct* 35 (19), 2429–2455.
- Pande, G. N., Liang, J. X., Middleton, J., 1989. Equivalent elastic moduli for brick masonry. *Comput Geotech* 8 (5), 243–265.
- Pau, A., Trovalusci, P., 2011. Block masonry as equivalent micropolar continua: the role of relative rotations. *Acta Mech* 223 (7), 1455–1471.
- Pietruszczak, S., Niu, X., 1992. A mathematical description of macroscopic behaviour of brick masonry. *Int J Solids Struct* 29, 531–546.
- Providas, E., Kattis, M. A., 2002. Finite element method in plane Cosserat elasticity. *Comput Struct* 80, 2059–2069.
- Ranganathan, S. I, Ostoja–Starzewski, M., 2009. Towards scaling laws in random polycrystals, *Int J Engn Sci* 47, 1322–1330.
- Sab, K., Nedjar, B., 2005. Periodization of random media and representative volume element size for linear composites. *CR Acad Sci II B* 333, 187–195.
- Salmi, M., Auslender, F., Bornert, M., Fogli, M., 2012. Apparent and effective mechanical properties of linear matrix-inclusion random composites: improved bounds for the effective behavior. *Int J Solids Struct* 49, 1195–1211.
- Sansalone, V., Trovalusci, P., 2010. Coupling continuum and discrete models of materials with microstructure: a multiscale algorithm. *Mater Sci Forum* 638–642, 2755–2760.
- Spence, S. M. J., Giofrè, M., Grigoriu, M. D., 2008. Probabilistic models and simulation of irregular masonry walls. *J Eng Mech–ASCE* 134, 750–762.
- Terada, K., Hori, T., Kyoya, T., Kikuchi, N., 2000. Simulation of the multi-scale convergence in computational homogenization approach. *Int J Solids Struct* 37, 2285–2311.

- Trovalusci, P., De Bellis, M., Ostoja-Starzewski, M., Murralli, A., Accepted. Particulate random composites as homogenized micropolar materials . *Meccanica*.
- Trovalusci, P., 2014. Molecular approaches for multifield continua:origins and current developments. In: Sadowsky, T., Trovalusci, P. (Eds.), *Multiscale Modelling of Complex Materials: phenomenological, theoretical and computational aspects*. Springer–Verlag, Berlin, CISM Courses and Lectures, Vol. 556.
- Trovalusci, P., Pau, A., 2014. Derivation of microstructured continua from lattice systems via principle of virtual works. The case of masonry–like materials as micropolar, second gradient and classical continua. *Acta Mech* 225, 157–177.
- Trovalusci, P., Varano, V., Rega, G., 2010. A generalized continuum formulation for composite materials and wave propagation in a microcracked bar. *J Appl Mech* 77 (6), 061002–1–11.
- Trovalusci, P., Capecchi, D., Ruta, G., 2008. Genesis of the multiscale approach for materials with microstructure. *Arch Appl Mech* 79, 981–997.
- Trovalusci, P., Masiani, R., 2005. A multi-field model for blocky materials based on multiscale description. *Int J Solids Struct* 42, 5778–5794.
- Trovalusci, P., Masiani, R., 2003. Non-linear micropolar and classical continua for anisotropic discontinuous materials. *Int J Solids Struct* 40, 1281–1297.
- Zeman, J., Šejnoha, M., 2007. From random microstructures to representative volume elements. *Model Simul Mater Sc* 15, S325–S335.